

WAKE FUNCTIONS FOR LAMINATED MAGNETS AND APPLICATIONS FOR FERMILAB BOOSTER SYNCHROTRON*

A. Macridin[†], P. Spentzouris, J. Amundson, Fermilab, Batavia, IL, USA
 L. Spentzouris, D. McCarron, Illinois Institute of Technology, Chicago, IL, USA

Abstract

The Fermilab Booster beam is exposed to magnet laminations, resulting in impedance effects much larger than resistive wall effects in a beam pipe. We present a calculation of wake functions in laminated magnets, which show large values at distances of the order of a few meters, but decrease quickly to zero beyond that. Therefore, strong in-bunch and nearest-bunch effects are present. We show realistic Synergia simulations of the Booster using these wake functions and space-charge solvers appropriate for the various geometries of the constituent elements of the machine. The simulation of tune shifts is in good agreement with experimental data. We find that wake fields in the Booster magnet laminations strongly increase beam emittance and have the potential to cause significant beam loss.

INTRODUCTION

Due to the high complexity of accelerators, simulations which employ large computers and sophisticated algorithms are required in order to understand and make predictions about beam dynamics. Besides high order maps to describe single particle propagation through accelerators, simulations should also consider collective effects such as space charge (SC) forces and wake field interactions. These problems can be addressed with the Synergia code developed at Fermilab [1]. Synergia is an extensible multi-language framework which incorporates a large collection of physical models, specialized modules and numerical libraries.

The Booster synchrotron is a 40 year old machine placed at near the beginning of the Fermilab accelerator chain, now typically running with beam intensities roughly twice the design value. Due to the strong demand for increasing intensity, investigation of collective effects in the Booster is of paramount importance.

A peculiarity of the Booster is the parallel-planes vacuum chamber formed by its laminated magnets [2]. Different authors stress the importance of wake effects in laminated structures [3, 4, 5, 6, 7]. While their analysis

is based on the analysis of impedance functions defined in frequency space, complex Synergia simulations require knowledge of distance dependent wake functions.

Recently, measurements of tune shifts in the Booster indicate the presence of quadrupole wake effects specific to geometries without circular symmetries [8]. While the quadrupole influence on the betatron tune shift has been discussed before in the context of resistive wall wakes [9], for Booster simulations it is important to study the effect in structures with laminations.

In the first part of the paper we calculate the impedance and wake functions for Booster laminated magnets. The wake fields are large and oscillate in sign at distances on the order of the bunch length, and decay quickly at large distances. This implies that in-bunch and nearest-neighbor-bunch wake interactions are predominant.

The second part shows results of Synergia simulations of the Booster at the injection energy. We find that the coherent vertical tune decreases with increasing beam intensity, while the horizontal tune is almost constant, in close agreement with experiment [8]. Synergia simulations also show that the wake has the potential to cause significant beam loss in Booster and strongly increases the beam emittance.

WAKE FUNCTIONS FOR LAMINATED MAGNETS

Formalism

The wake functions describe the effect of the electromagnetic field created by a particle moving through an accelerator beam pipe upon the trailing particles. We consider a parallel-planes beam pipe as a suitable approximation for the Booster magnets. If the distance between the leading and trailing particle is $|z|$, the momentum of the trailing particle traversing a structure of length L will be modified by:

$$c\Delta p_z = -qQW^{\parallel}(z) \quad (1)$$

$$c\Delta p_x = -qQ(W_x^{\perp}(z)X - W_x^{\perp}(z)x) \quad (2)$$

$$c\Delta p_y = -qQ(W_y^{\perp}(z)Y + W_y^{\perp}(z)y) \quad (3)$$

Here Q (q) and (X, Y) ((x, y)) represent the charge and the transverse displacement of the leading (trailing) particle respectively. \parallel and \perp denote the longitudinal and the transverse directions. The higher order terms in the displacement are neglected. For this particular geometry, only two wake functions, $W_x^{\perp}(z)$ and $W_y^{\perp}(z)$, are needed for the transverse directions (Eq. 2 and Eq. 3). This is a con-

* This work was supported by the United States Department of Energy under contract DE-AC02-07CH11359 and the ComPASS project funded through the Scientific Discovery through Advanced Computing program in the DOE Office of High Energy Physics. This research used resources of the National Energy Research Scientific Computing Center, which is supported by the Office of Science of the U.S. Department of Energy under Contract No. DE-AC02-05CH11231 and of the Argonne Leadership Computing Facility at Argonne National Laboratory, which is supported by the Office of Science of the U.S. Department of Energy under contract DE-AC02-06CH11357.

[†] macridin@fnal.gov

sequence of the translational symmetry along the horizontal direction and of the Panofsky-Wenzel theorem which requires that $\frac{\partial \Delta p_x}{\partial x} = -\frac{\partial \Delta p_y}{\partial y}$. The terms proportional to the displacement of the leading particle, i.e., to X or Y , are called *dipole* wakes while the ones proportional to the displacement of the trailing particle, i.e., to x or y , are called *quadrupole* wakes. Note that in a circular pipe, the quadrupole wake fields vanish due to symmetry.

To calculate the electromagnetic field, often it is easier to solve the Maxwell Equations in the frequency domain, and afterward calculate the impedances. Once the impedances are known the wakes can be obtained by a Fourier transform,

$$W^{\parallel}(z) = \frac{1}{2\pi} \int d\omega Z^{\parallel}(\omega) e^{-j\frac{\omega}{c}z} \quad (4)$$

$$W_{(x,y)}^{\perp}(z) = \frac{j}{2\pi} \int d\omega Z_{(x,y)}^{\perp}(\omega) e^{-j\frac{\omega}{c}z}. \quad (5)$$

Next we describe how to calculate the wake functions for a beam pipe with parallel faces formed by laminated magnets. First the impedances are calculated and then the wake functions are obtained via Eq. 4 and Eq. 5. The calculation of the impedance for laminated magnets closely follows Ng's derivation [3]. Since the wake is the Fourier transform of the impedance, is important to have accurate knowledge of the impedance at all frequencies.

The electromagnetic field inside a pipe with finite conductivity can be seen as a sum of two terms, one being the solution of the beam inside a pipe with the same geometry but with infinite conductivity and the rest. The first contribution to impedance is proportional to γ^{-2} , thus vanishing in the relativistic limit. The second contribution, referred to as the coupling impedance, is produced by currents in the pipe walls and is a consequence of their finite conductivity. We approximate it in our simulations with the solution of the Maxwell Equations for a relativistic beam in a pipe with finite conductivity. Since the Fermilab Booster, with a gamma of 1.4, is away from the relativistic limit, we account for the first term by employing numerical solvers for perfect conductors and grounded chambers.

We first focus on the solution in a pipe formed by two parallel metallic plates at distance $2b$ from each other. The impedances in this case can be written, to a good approximation [3], as a function of \mathcal{R} :

$$Z^{\parallel} = \frac{\mathcal{R}}{2\pi b}, \quad (6)$$

$$Z_x = \frac{\mathcal{R}}{2\pi k} \int_0^{\infty} d\eta \frac{\eta^2 \operatorname{sech}^2 \eta b}{1 - \frac{j\mathcal{R}\eta}{Z_0 k} \tanh \eta b}, \quad (7)$$

and

$$Z_y = \frac{\mathcal{R}}{2\pi k} \int_0^{\infty} d\eta \frac{\eta^2 \operatorname{csch}^2 \eta b}{1 - \frac{j\mathcal{R}\eta}{Z_0 k} \coth \eta b}, \quad (8)$$

where \mathcal{R} is the longitudinal surface impedance at the pipe walls $E_z = \mathcal{R}H_x|_{y=\pm b}$. For a metallic pipe, over a large

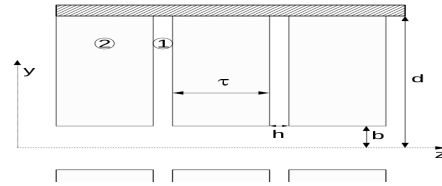


Figure 1: Parallel-faced beam pipe with laminations. Subscripts "1" and "2" denote the crack and lamination, respectively. The laminations are shorted by an ideal conductor "3".

range of frequencies, $\mathcal{R}(\omega) = \frac{1+j}{\delta\sigma}$, where $\delta = \sqrt{\frac{2}{\omega\sigma\mu}}$ is the penetration depth of the electromagnetic field inside the pipe wall and μ is the magnetic permeability. $Z_0 \approx 377\Omega$ is the free space impedance and $k = \frac{\omega}{\beta c}$ is the longitudinal wave number which defines beam propagation.

The parallel-plate pipe geometry with laminated magnets is sketched in Fig. 1. The subscript "1" denotes the dielectric crack of width h and "2" denotes the metallic lamination of width τ . In our model the laminations are shorted by an ideal conductor "3" at distance d from the pipe center.

Once the surface impedance \mathcal{R} of the pipe with laminations is known, one can use equations 6, 7 and 8 to calculate the impedances. Following [3] and [4], we consider

$$\mathcal{R} = \frac{\mathcal{R}_c h + \mathcal{R}_l \tau}{h + \tau} \approx \frac{\mathcal{R}_c h}{h + \tau}, \quad (9)$$

where $\mathcal{R}_l = \frac{1+j}{\delta_2 \sigma_2}$ is the lamination surface impedance and \mathcal{R}_c is the crack surface impedance. The crack surface impedance can be written as [3]

$$\frac{\mathcal{R}_c}{Z_0} = \frac{j q}{\omega \epsilon_1} \tan q(d - b) \quad (10)$$

where

$$q^2 = k_1^2 \left(1 + \frac{\mu_2 \delta_2}{\mu_1 h} (1 - j) \tanh(g_2 \frac{\tau}{2}) \right), \quad (11)$$

with $g_2 \approx \frac{1+j}{\delta_2}$ and $k_1 = \frac{\omega \sqrt{\epsilon_{r1} \mu_{r1}}}{c}$. The term $\tanh(g_2 \frac{\tau}{2})$ in Eq. 11 accounts for the finite value of the lamination width and was not considered in [3].

Impedance and Wake Functions in Booster

There are two kinds of laminated magnets in the Booster, combined function focusing (F) and defocusing (D) magnets, characterized by $d = 15.24 \text{ cm}$, $h = 9.52 \times 10^{-4} \text{ cm}$, $\tau = 6.35 \times 10^{-2} \text{ cm}$, $\epsilon_{1r} = 4.75$, $\mu_{2r} = 100$, and $\sigma_2 = 0.5 \times 10^7 (\Omega m)^{-1}$ (iron). The F-magnet has $b = 2.1 \text{ cm}$, while the D-magnet has $b = 2.9 \text{ cm}$. We show results for the F-magnet. Those for the D-magnet are similar.

In Fig. 2 we illustrate the longitudinal and the transverse impedances for the F-magnet. At low frequency the current is circulating around the crack through the iron laminations, thus covering a distance of approximately $2(d - b)$

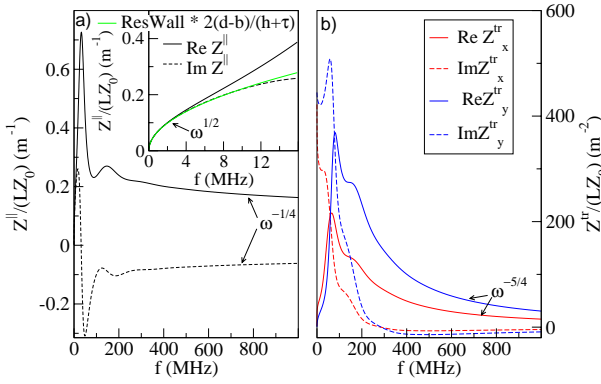


Figure 2: Impedances in the Booster F-magnet. a) Longitudinal impedance. Notice (inset) that at low frequencies the impedance has a $\omega^{1/2}$ behavior characteristic of resistive wall pipes, but is $2\frac{d-b}{h+\tau} \approx 385$ larger than the corresponding impedance of an iron pipe. b) Transverse horizontal and vertical impedances.

between two neighboring cracks, while the cracks are located at distance $h + \tau$ on z-axis. Therefore, as shown in Fig. 2a the low frequency behavior of Z^{\parallel} is proportional to $\omega^{1/2}$ and characteristic of resistive wall pipes. However, it is much larger (about $2\frac{d-b}{h+\tau} \approx 385$ times larger, see inset) than the corresponding impedance of an iron pipe. At larger frequencies the behavior changes completely. In the interval $20\text{ MHz} \simeq 400\text{ MHz}$, which is of the order of the bucket length¹, Z^{\parallel} is large and displays two peaks. At large frequency the longitudinal impedance shows $\omega^{-1/4}$ behavior, characteristic of laminated structures [3, 4]. The transverse laminated impedances (Fig. 2b) are also large compared to the corresponding frequencies for the resistive wall case. They are strongly peaked around $60\text{ MHz} \simeq 80\text{ MHz}$. At smaller frequencies, the real part of the vertical impedance is smaller than the horizontal one, whereas at larger frequencies, it is about two times larger, a behavior characteristic of parallel-plane geometry [10]. The large frequency asymptotic behavior of the transverse impedance is $\omega^{-5/4}$.

Fig. 3 shows the wake functions calculated via Fourier transform from the impedances plotted in Fig. 2. For comparison, the resistive wall impedance for an iron beam pipe is also illustrated. The magnitude of the longitudinal and transverse wake functions for an F-magnet are much larger (about 2 orders of magnitude) than the resistive wall wakes at a distance of the order a few meters. They have also a very different shape in this distance interval, oscillating in sign. For $|z| < 2\text{ m}$ the vertical transverse wake is two times larger than the horizontal wake, but for $|z| > 10\text{ m}$ it becomes smaller. Compared to the resistive wall transverse wake which goes like $|z|^{-0.5}$, we find that the F-magnet horizontal wake decreases as $\approx |z|^{-1.22}$, which is much faster (the asymptotic behavior of the D-magnet horizontal wake is $\approx |z|^{-1.23}$).

¹In Booster, at injection, the bucket length is 5.64 m.

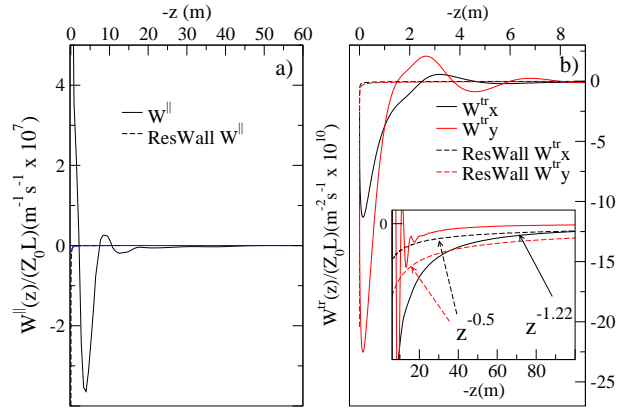


Figure 3: Wake functions for a Booster F-magnet and a resistive wall iron pipe. a) Longitudinal wake function versus the distance $-z$. For $|z| < 2\text{ m}$ the wake is strongly repulsive, while around $|z| \approx 4\text{ m}$ it has a large attractive peak. For $|z| > 10\text{ m}$ the longitudinal wake is also attractive. b) Transverse horizontal and vertical wake functions. The wake functions are large at distances of order meters and decay quickly at large distance. Note (inset) that for $|z| > 100\text{ m}$ ($|z| > 10\text{ m}$) the horizontal (vertical) impedance for an F-magnet becomes smaller than for the resistive wall pipe. Whereas the transverse resistive wake behaves as $|z|^{-0.5}$ for large $|z|$, the horizontal wake for an F-magnet decreases as $|z|^{-1.22}$.

The long distance behavior of the horizontal transverse wake is important for the quadrupole coherent tune shift characteristic to geometries without circular symmetry[9]. The quadrupole tune shift is a consequence of the quadrupole wakes described in Eq. 2 and Eq. 3. It can be a substantial effect for wakes which persist for long distances, such as the $|z|^{-1/2}$ resistive wall wake, since it can accumulate the contribution of many previous turns. However, the accumulation effect of previous turns on the quadrupole tune shift is less important for laminated magnets. The large value of laminated wakes at small distance shows that in-bunch and nearest-neighbor-bunch interactions are the most important. As discussed in the next section, we also find that the large and repulsive longitudinal wake at distance $< 2\text{ m}$ can be responsible for beam loss.

SYNERGIA AND BOOSTER RESULTS

Synergia and Booster Modeling

Synergia is a multi-language extensible framework utilizing state-of-the-art numerical libraries, solvers, and physics models, being designed to model beam dynamics in accelerators. Synergia features 3D SC solvers, impedance modules and arbitrary order Lie maps for magnetic optics. A detailed description of Synergia can be found elsewhere [1].

In order to model the Booster we developed new 3D SC solvers suitable for parallel-planes and rectangular vacuum

chambers for Synergia. We also developed new modules to simulate the laminated wake fields described in the previous section. The Booster has 24 cells, each cell including F-magnets and D-magnets and circular pipe drift sections [2, 8]. For each of these constituent elements we consider suitable wake field and SC solvers.

The SC solvers used in the simulations treat the vacuum chambers as ideal conductors. Thus image charges and image currents are always included when we talk about SC effects in our simulations. These effects are important since we present simulations at injection energy of 400 MeV ($\gamma = 1.42$), quite far from the relativistic limit.

The simulation is initialized with a six-dimensional Gaussian beam matched for propagation without collective effects. The input parameters are $x_{rms} = 0.0086 m$, $y_{rms} = 0.0032 m$ and $z_{rms} = 0.88 m$. Different beam intensities of up to 6×10^{12} particles are considered. These values are similar to those in the Booster during the experimental runs [2]. Since the experimental data was taken at the injection energy, in the simulations the phasing of the rf cavities is set up so that there is no net acceleration of the beam. To determine the coherent tunes, we measure the position of the beam center at different locations over 1000 turns. The tunes are extracted from the Fourier transform of the beam center displacement as a function of position.

Results

In order to investigate and minimize the role played by the coupling between the horizontal and vertical motion in the Booster on the tune shifts, measurements with different base tunes (i.e. tunes at small intensity) were performed. The base tunes can be modified by changing the current settings of the quadrupole correction magnets. Analogously, we can change the base tunes in our simulations. We employed simulations for different base tunes and, in agreement with experimental measurements [8], we also find that the horizontal-vertical coupling does not play a significant role in tune shift analysis.

In Figs. 4a and 4b, simulation of the coherent betatron tune shifts in the horizontal and vertical planes are compared with the experimental data [8] (black circles). Notice that the scale for the vertical tune shift is about 20 times larger than for the horizontal one. A train of 84 bunches, i.e. the full Booster machine, is considered. In order to better understand the contribution of SC and the coupling impedance several cases were studied. The red circles are the results of the simulations which include both SC and coupling wake fields. The agreement with the experimental data is good. The vertical tunes are decreasing with intensity. However, we find that the calculated slope (-0.012 per 84×10^{10} particles) is a little larger than measured (-0.009 per 84×10^{10} particles). As in the experiment, we find that the horizontal tunes do not change significantly with beam intensity, the slope being near zero within the error bar. The blue circles show the results when only the coupling wake is considered, while the green squares

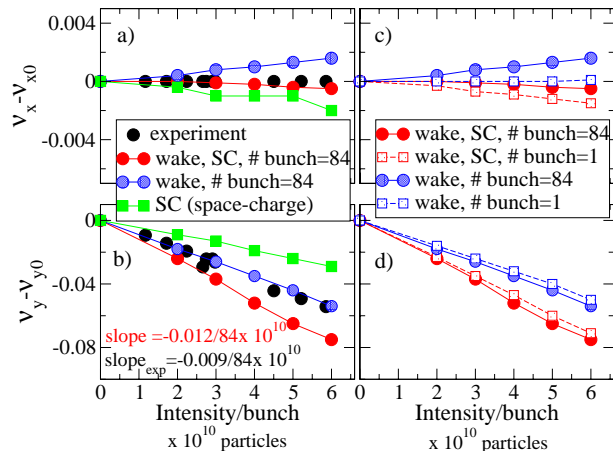


Figure 4: Coherent tune shift versus beam intensity. The estimated tune uncertainty is less than 0.001. a) & b) Comparison with experiment, full machine simulations. The vertical tune is suppressed while the horizontal tune changes very little. Space charge (SC) suppresses both the vertical and horizontal tunes, while the wake coupling suppresses the vertical tune and increases the horizontal tune. c) & d) Single and multi-bunch calculations. The effect of the multi-bunch wake interaction is small, although it enhances the decrease (increase) of the vertical (horizontal) tune.

show the case when only the SC interaction is taken into account. For the vertical case, both the wake and the SC force decrease the tune, the coupling wake having a larger effect. For the horizontal case, the SC force suppresses the tune, while the wake increases it. However, both effects are small. The latter is due to the quadrupole contribution which is expected to increase the horizontal tune [9].

We find that the effect of the multi-bunch wake interaction on the tune shift is small. In Figs. 4c and 4d we compare single-bunch (squares) and multi-bunch (full machine, circles) simulations. Simulations with (red symbols) and without (blue symbols) SC are shown. The decrease of the vertical tune and the increase of the horizontal tune is enhanced when multiple bunches are considered. However, the effect is small, about 10% for the vertical tune and close to the resolution for the horizontal tune.

Interesting features of wake fields effects are seen in the longitudinal phase space beam profile. We find that the wake field is responsible for beam loss. In Fig. 5a and 5b the longitudinal beam profiles at injection and after 1000 turns are shown. SC, wakes fields and multi-bunch interactions are considered. During propagation, see Fig. 5b, a significant fraction of particles (red points) departs the region inside the separatrix ($\approx 0.8\%$ after 1000 turns) and thus will finally get lost. By tracking back to the initial position of the lost particles one sees in Fig. 5a that these particles (red points) were initially located in the vicinity of the separatrix.

The multi-bunch wake interaction reduces beam loss.

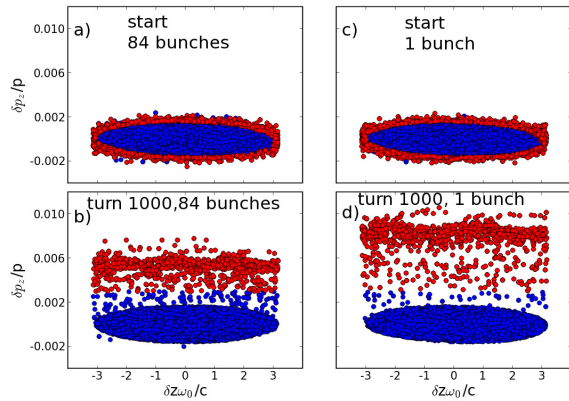


Figure 5: Beam profile in the longitudinal phase space defined by $(\delta z \frac{\omega_0}{c}, \frac{\delta p_z}{p})$, where ω_0 is the cavity rf. 5×10^{10} particles/bunch. The particles close to the separatrix at injection are susceptible to beam loss (red points). a) & b) Full machine. $\approx 0.8\%$ beam loss after 1000 turns. c) & d) Single bunch. $\approx 1\%$ beam loss after 1000 turns.

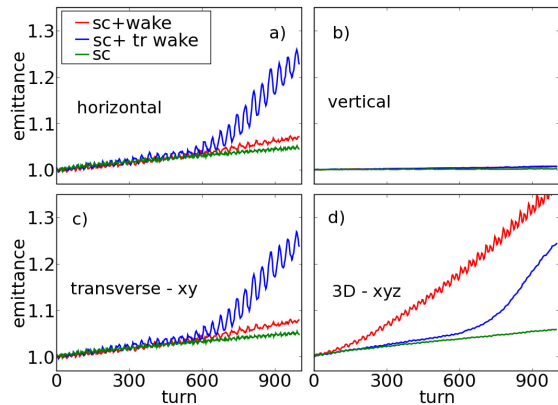


Figure 6: Emittance versus turns. 5×10^{10} particles/bunch. Simulations with SC and full wakes (red), with SC and only transverse wakes (blue) and with only SC (green). a) Horizontal. b) Vertical. c) XY-plane. d) Full 3D emittance. The transverse wakes increase the transverse emittance.

That can be inferred from comparing Fig. 5b with Fig. 5d where a single bunch simulation is shown. In the single bunch simulations the particles starting in the vicinity of the separatrix depart faster. Compared to multi-bunch simulations, more particles get lost ($\approx 1\%$ after 1000 turns compared to $\approx 0.8\%$). The fact that multi-bunch interaction stabilizes the beam and helps reduce beam loss can be understood from the shape of the longitudinal wake (see Fig. 3a). At distances relevant for in-bunch interaction the wake is large and repulsive (up to $\approx 2 m$), while it becomes attractive at distances of order of the bucket length ($= 5.64 m$) relevant for the nearest-neighbor bunch interaction. At large distances, above $\approx 10 m$, the wake is also attractive. The bunch-bunch attraction reduces beam loss.

In Fig. 6 we show the beam emittance evolution. The

emittance is calculated as the determinant of the beam covariance matrix in the phase space. The 3D-emittance (Fig. 6d, red line) increases strongly in the presence of the wake fields. If the longitudinal wake and therefore the beam loss effect are suppressed, the transverse wakes still increase the emittance (blue line), especially in the horizontal plane (Fig. 5a). The SC effect on the emittance increase is small, as seen from the simulations with the wake fields turned off (green line). The vertical emittance is not affected much by neither wake fields nor SC (Fig. 5b).

CONCLUSIONS

We discussed the calculation of impedance and wake fields in laminated magnets with parallel-planes geometry suitable to describe Booster magnets. Synergia simulations including both SC and wake fields appropriate for the constituent elements of the Booster machine were employed.

The coupling impedances for laminated magnets in Booster are large and peaked at frequencies which correspond to distance of the order of the bunch size. The corresponding wake functions are also large and oscillate in sign at distances relevant for in-bunch and neighboring-bunch interactions. At large distances the transverse wakes decay faster than the similar resistive wall wake functions. Therefore the effect of the quadrupole wake is less important as the number of revolutions around the machine accumulate.

Simulations at the injection energy show that the coherent vertical tune decreases with increasing beam intensity while the horizontal tune is almost constant, in good agreement to the results obtained by experiment. Both the SC force and the wake fields reduce the vertical tune. While the horizontal tune is suppressed by the SC, the wakes increase it. Wake interactions between neighboring bunches give only a small contribution to the tune shifts.

The effect of SC force on the beam emittance is small for the simulated period of time, whereas the wake fields strongly increase the emittance. Aside from the beam loss effect caused by the longitudinal wake, the transverse wakes significantly increase the horizontal emittance.

REFERENCES

- [1] J. Amundson, P. Spenzouris, J. Qiang, R. Ryne, J. Comp. Phys. 211, 229 (2006).
- [2] Booster Rookie Book, Fermilab, www-bdnew.fnal.gov/operations/rookie_books.
- [3] K. Y. Ng, Fermilab FN-0744, (2004).
- [4] R. Gluckstern, Fermilab Report, TM-1374, (1985).
- [5] A. G. Rugeira, Fermilab Report, FN-219, (1970).
- [6] A. G. Rugeira, Fermilab Report, FN-220, (1971).
- [7] S. C. Snowdon, Fermilab Report TM-277 (1970).
- [8] Daniel McCarron, Ph. D. Thesis, Fermilab, 2010.
- [9] A. Chao, S. Heifets and Bruno Zotter, Phys. Rev. STAB, 111001 (2002).
- [10] A. Burov and V. Lebedev, Proceedings of EPAC-2002, 1445, (2002).